Study of Acoustic Emission Signals During Crack Propagation in Multiscale Nano-Composites

Sharath P. SUBADRA*, Tomaž KEK**, Zoran BERGANT**, Paulius GRIŠKEVIČIUS*

*Faculty of Mechanical Engineering, Kaunas University of Technology, Studentų g. 56, 51424 Kaunas, Lithuania, E-mail: sharadhsub@outlook.com, paulius.griskevicius@ktu.lt

***Faculty of Mechanical Engineering, University of Ljubljana, Aškerčeva cesta 6, 1000 Ljubljana, Slovenia*

1. Introduction

Multiscale nano-composites have been reported to have enhanced toughness especially with the use of nano-tubes. Nano-materials tend to arrest the growth of crack when loaded. An increase of 8.5% in stiffness was reported with the addition of nano-fillers in the matrix [1]. Similar results were obtained by Ashish Warrier et.al when CNTs where used in both the matrix and the sizing [2]. Thus it could be said with fair amount of confidence that, a genuine increase in mechanical properties-fracture toughness, inter-laminar shear strength-is observed when CNTs are either deposited on the fibre or dispersed in the matrix. The degree to which these properties are improved depends on a variety of factors like the way in which CNTs are integrated in the composites-like growing on fibres, mixed in the resin, added to fibre sizing, type of CNTs, surface functionalization, toughness of base matrix etc. [3]. The enhancement of fracture toughness in polymer composites depends on the length of the CNTs. The bridging process could either be due to the CNT pull-out or CNT rupture. In either of the cases the nanotubes bridge the crack surface, thereby shielding the crack front from carrying the entire tensile load [4]. Thus, from these positive developments reported, nanotubes formed an essential part of this study. Crack propagation can be considered as an ultimate form of failure mechanism, which takes place in the inter-laminar zone during de-lamination. Since it can be evaluated visually it could be considered as a macroscopic failure activity. Microscopic phenomena leading to de-lamination such as fibre rupture, matrix cracking etc. could be monitored by acoustics emissions [5–9]. AE is an efficient method to monitor in real time the damage growth in structural components and laboratory specimens. In loaded materials, strain-energy release due to micro-structural changes results in stress wave propagation. In composite materials many mechanisms have been confirmed to produce AE signals which includes matrix-cracking, fibre-matrix interface de-bonding, fibre breakage and de-lamination. AE deals with the detection of such waves at the surface of the material. Thus, this technique allows not only to determine the location of the source of the emission but also helps in determination of its nature [9].

1.1. Theory of modal acoustic emission

Modal acoustic emission theory considers the AE signals to be dispersive elastic waves. The propagation of elastic waves in thin-walled structure exhibits multi-modes and dispersion characteristics [10]. An analysis of these modes provides some insight into the damage types the composites undergo. The plate theory corroborates that the acoustic waves propagates through plates in two different modes, the symmetric "S0" mode and the anti-symmetric "A0" mode Fig. 1 [11]. With reference to [11] it could be further said that, when AE waves travel in flat plates they exhibit a different behaviour attributable to the bounded surface of the structure. The waves are bounded by the surface and are subjected to wave-guide effect, thereby causing them to propagate as Lamb waves. As mentioned above these waves propagate in two distinctive modes namely, longitudinal waves, in the plane of the surface, and transverse waves, perpendicular to the surface [12].

From the figure below it could be inferred that AE signal energy is present in portions of both the modes. This illustrates a key advantage of Wavelet Transforms-WT over Fast Fourier Transforms-FFT. WT shows how the signal energy is distributed as a function of frequency, time and mode whereas FFT provides only the frequency content of the whole signal [13].

Delamination in composites are largely associated with the production of mechanical displacement micro-pulses outside the plane (OP), while matrix micro-cracking and fibre breakage may produce micro-pulses inside the plane (IP). It has been understood that A0 mode is favoured by OP excitations and S0 by the IP excitations [13]. In a study conducted by Y. Mizutani et.al, it was understood that fibre fracture was characterised by the presence of both S0 and A0 modes, with energy concentration in the S0 mode at a frequency range of 200-400 kHz. Matrix cracking (transverse) when viewed in the wavelet contour was found to have a component around 300 kHz. Since low frequency component were absent, signals appeared in a single mode namely S0 mode. Delamination was, like fibre fracture characterised by two modes, and the wavelet contour showed that both modes S0 and A0 had strong high frequency content. Fibre and matrix de- bonding was characterised by low frequency A0 mode. The material used in this study was carbon fibre reinforced composites subjected to point load. In another study conducted by Christopher Baker et.al, similar results were obtained in the case of matrix cracking both surface and internal [14]. Comparing the studies mentioned in [12–14], a table is compiled elaborating the kind of modes to be expected when a composite specimen undergoes failure and is shown below.
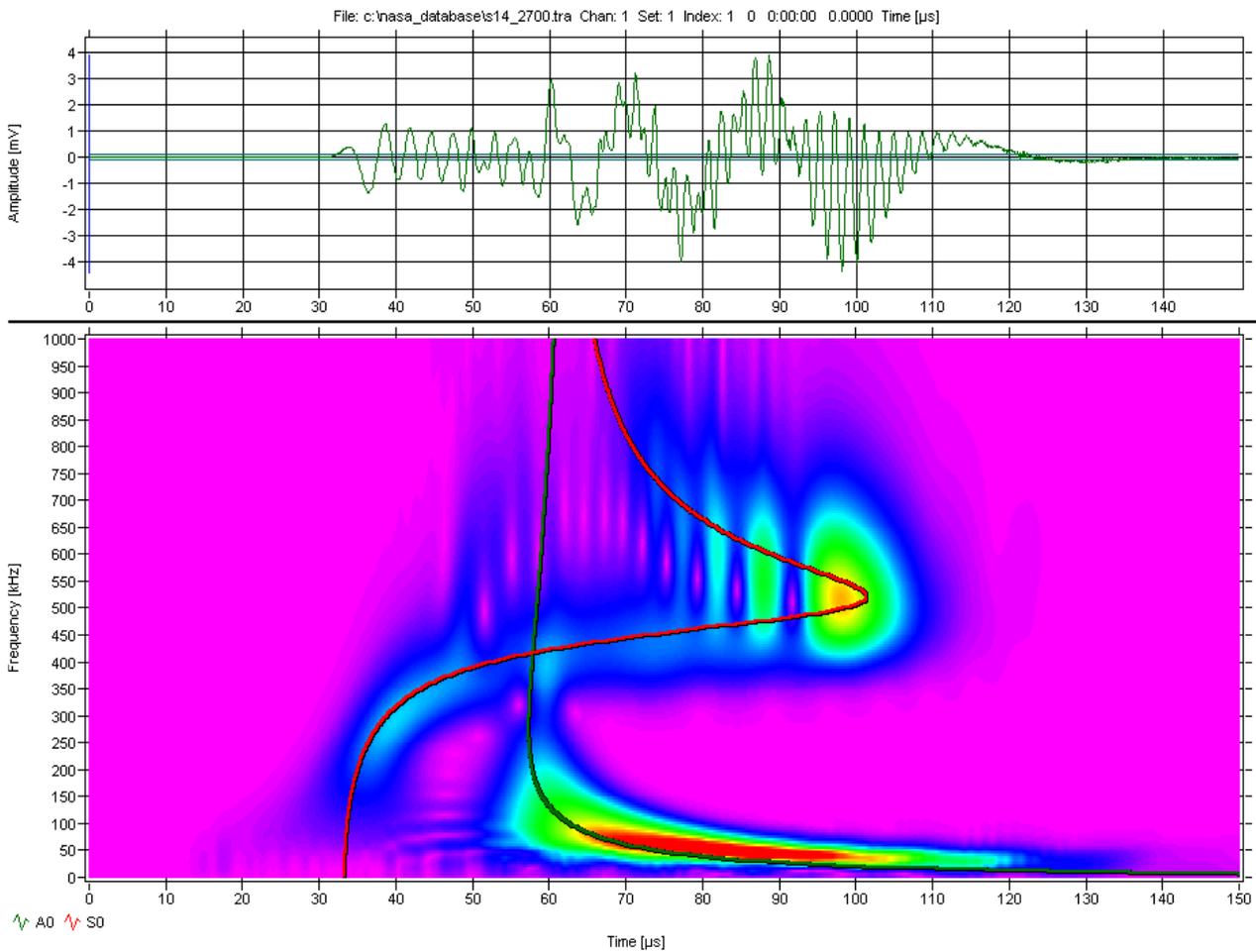
Fig. 1 Calculated AE signals from an in-pane dipole source with corresponding WT (Wavelet Transforms) with super-imposed modes. On the x-coordinate we have time in µs and on the y-coordinate we have frequency in kHz [11]

Table 1

Modes expected from the failure mechanism of carbon fibre reinforced composites

FRACTURE MECHANISM	LAMB WAVE MODES	FREQUENCY MODES	DESCRIPTION
Fibre fracture	Predominantly S0 mode along with A0 mode	S0 300~500 kHz	Wavelet contour had both A0 and S0 modes, but usually S0 mode prevails
Matrix cracking	S0 and A0 mode	S0 ~300 kHz A0 ~100 kHz	Surface crack excites A0 mode while internal cracks excites S0 mode
De-lamination	S0 and A0 mode	Both the modes has higher frequency content	Both the modes usually have higher frequency content
Fibre-matrix de-bonding	A0	Characterised by low frequency A0 mode	Characterised by low frequency A0 mode

This Table 1 would be used as a reference for further analysis on the acoustic signals obtained for the specimens used in this work. This wouldn't be used as an absolute reference since in all these tests, the loads applied were either a tensile force or a bending test. While in our case we had double cantilever beam specimens and the crack opening mode was simulated. No literature specifically illustrates the kind of signal one should expect when we have this kind of loading.

2. Experimental

2.1. Material

The materials used in this study includes carbon fibre, an epoxy material with hardner and multi-walled carbon nano-tube (MWCNTs). The MWCNTs were procured form "FIBREMAX COMPOSITES" a Greek supplier of composite materials. The specifications of the MWCNT are; Bulk volume 4 lt; Average diameter 10-40 nm; Length 1-25 µm; Purity by weight 93% min and Specific surface area 150-250 m^2/g. The epoxy material along with the hardner was procured from "R&G Faserverbundwerkstoffe GmbH". As per the manufacturers claim this resin system (Epoxy resin L+Hardner GL2) offers an approval by the *Germanische Lloyd* for the construction of the boats and rotor blades for wind turbines. Thus this resin system has the following properties; low viscosity, highly transparent, fully cures at 15°C, glass transition temperature Tg>85°C, Pot life (time taken for an initial mixed viscosity to double or quadruple for lower viscosity products) of approximately 210 minutes, high static and dy-

namic strength. The various mechanical properties of the resin system are as follows; Density 1,151 g/cm³, tensile strength 74,8 MPa, elongation at break 4,5%, tensile modulus 3057 MPa, flexural strength 119 MPa. A 0.1 thick polyester was used as de-lamination initiator inserted in the centre plane of the laminates. Both sides of the film were coated with mould release agent to minimise adhesion between the film and the matrix material of the composite material.

Carbon fibres where used in this work, which are of the non-crimp type. The fibres (commercial name: PY-ROFILTMTR505 15K) were procured from "R&G Faserverbundwerkstoffe GmbH". As per the manufacturers catalogue the fibre has the following properties; Modulus 240 GPa, tensile strength 4900 MPa, elongation at break 2%, density 1,82 g/cm³ and areal density of 200 g/m².

Wet-lay-up technique was adopted to prepare the panels. Two set of specimens where prepared; the first set numbering three (1.n, $n=1,2,3$) contains no CNTs in the matrix material, while the second set numbering three (2.n) has 0.3 wt% of nanotubes in the matrix material (the CNTs where hand stirred into the matrix in a vacuum chamber). Latter the specimens where cut as per ASTM D 5528[15]. The fibre volume fraction was calculated using the relation:

$$V_f = \frac{Nm}{h\rho_f},$$ (1)

where: N is the number of plies, m the areal density, ρ_f is density of fibres and h is the thickness of the specimens [3]. Fig. 2, a and b shows the specimens that were used in this work. Table 2, shows detailed specimen dimensions and other details.
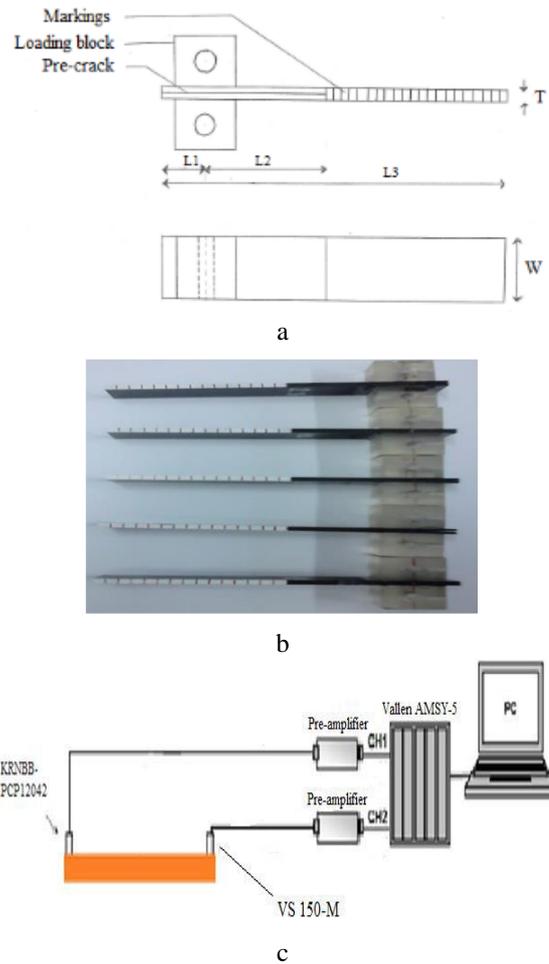
Fig. 2 Specimen as per ASTM 5528-01 – a. Specimen with an edge painted white to aid visual detection of de-lamination, the black lines are 5 mm apart – b. Experimental setup – c

Table 2

Specimen dimensions, along with the masses and fibre volume fraction.

Sl No.	L1 (mm)	L2 (mm)	L3 (mm)	W (mm)	T (mm)	T1 (without foil)	Mass (g) ± 0.1g	Mass (g) ± 0.0001g	Mass-foil (g)	Mass-no foil (g)	Fibre volume fraction (%)
1.1	18.75	50.08	142.81	24.98	3.82	3.72	19.7	19.6370	0.2370	19.4000	53.17
1.2	17.51	50.23	142.78	24.97	3.76	3.66	19.6	19.5500	0.2330	19.3170	53.97
1.3	18.46	50.42	142.78	25.04	3.77	3.67	19.5	19.4532	0.2380	19.2152	53.89
2.1	17.58	49.95	142.33	25.06	3.78	3.68	19.4	19.3199	0.2340	19.0859	53.75
2.2	18.28	50.03	142.22	24.88	3.78	3.68	19.5	19.4730	0.2350	19.2380	53.75
2.3	17.5	49.9	142.43	24.96	3.80	3.70	19.6	19.5626	0.2320	19.3306	53.46

2.2. Mode-I inter-laminar crack propagation test

The specimens were loaded on a 50 kN capacity servo-drive controlled screw driven load frame. The opening forces were applied to the DCB specimen with loading blocks glued on both side of the specimen as shown in Fig. 2, c, the specimen is given a colour in the picture. The end of the DCB is opened by controlling the crosshead movement. The tests were carried out with a displacement speed of 5 mm/min, while the load and delamination length were recorded.

Acoustic signals were captured when the specimens where subjected to loading. A Vallen-Systeme GmbH acoustic emission measurement system AMSY-5 (Vallen-Systeme GmbH, Icking, Germany) was used to capture and analyse the AE signals at 5 MHz sampling frequency. Two sensors namely a piezoelectric AE sensor VS150-M with a measuring range between 100 and 450 kHz and resonance at 150 kHz and a SteveCo KRNBB-PCP12042 wide band sensor with a frequency ranging from 100 kHz to 2.5 MHz were used. The sensor connections is as shown in Fig. 2, c. The amplitude threshold was set up at 40 dB. The entire process was recorded on a camera to calculate the inter-laminar fracture toughness.

2.3. Determination of inter-laminar toughness

As per the ASTM 5528-01[15] three methods are available for determination of determination inter-laminar

fracture toughness and they are; Modified Beam Theory (MBT), Compliance Calibration method (CC) and Modified **C**ompliance **C**alibration method (MCC). The modified beam theory was used to determine the inter-laminar toughness as it gave a more conservative value.

The beam theory expression for strain energy release rate of any perfectly built-in double cantilever beam is given by the following expression:

$$G_j = \frac{3P\delta}{2ba},$$
(2)

where: P is the applied load, δ is the load point displacement, b is the specimen width, and a de-lamination length. But in practise the above equation doesn't hold good since all beams are not perfectly built in. Hence we correct this by adding an absolute value of Δ to de-lamination length thus treating the DCB, as if it contained a longer de-lamination. Thus the above equation can be modified by incorporating $|\Delta|$. As P reaches its critical value P_C, the crack starts propagating. The corresponding G_I value would be critical energy release rate G_{Ic} and this is a material characteristic that represents the fracture toughness of the cracked interface. Based on an energy criterion, G_{Ic} gives an estimation of the amount of energy absorbed during crack growth [5].

$$G_j = \frac{3P\delta}{2b(a + |\Delta|)}.$$
(3)

3. Results and discussion

3.1. Mechanical performance

Fig. 4 details the influence of CNTs on the mechanical performance of the material. The figure below (Fig. 4, a) was obtained while studying the mode-I inter-laminar fracture toughness of the DCB specimens. As seen in the figure there is an increase in load for all the specimens and the slopes are similar due to the same pre-crack length used in all of them. This gradual increase in load was followed by a sudden decrease which marks the initiation of crack. It was observed that after this initial drop the load increased considerably but lesser than the previously attained maximum loads in all the specimens studied. For instance in specimen 1.1 the load increased upto 113N before dropping to 103N, but latter increased to 111N. The abrupt load decrease was earlier in case of specimens without CNTs (1.1, 1.2, and 1.3) while those with CNTs (2.1, 2.2, and 2.3) the load decrease was found in a later stage. For instance if specimen 2.1 is considered, though initially there was a load decrease as in all specimens but this decrease was not as abrupt as in the 1.n (1.1, 1.2 and 1.3) series. After an initial negligible drop from a maximum of 98.15 N to 94 N, there was a gradual decrease of load and later a gradual increase in load with intermediate negligible load drops until it reached a maximum of 92 N. From this it could be inferred that an external hardening was provided by the CNTs either through fibre pull outs or bridging. This phenomena was not observed in the case of 1.n series. In these specimens the curve looked rather unstable. But, these specimens could withstand much higher loads before initiation of crack when compared to those

with CNTs. From this it could be inferred that there is a considerable degradation in either the mechanical or chemical properties of the matrix material.
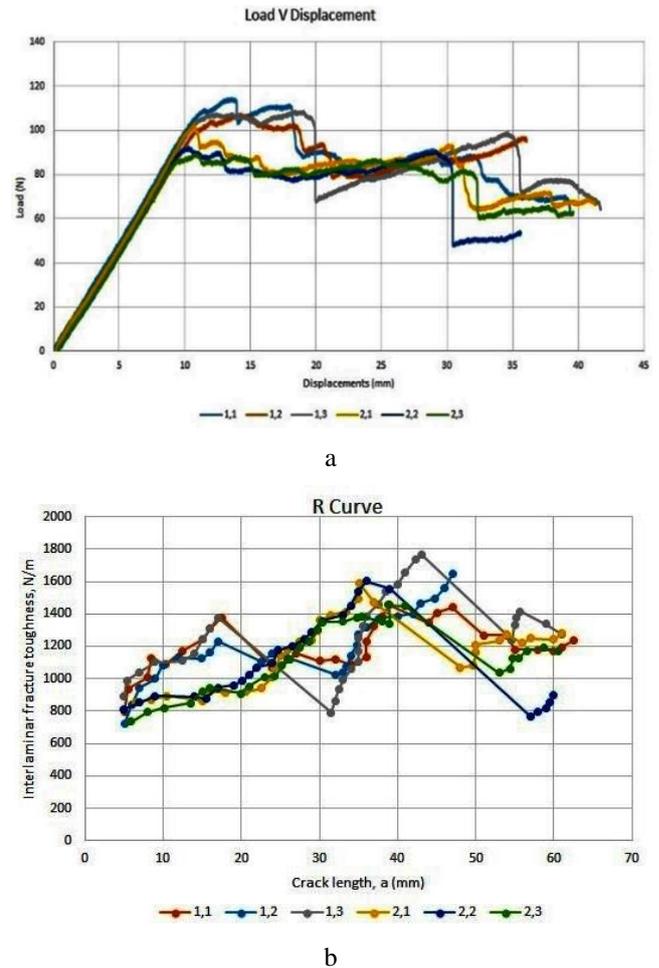

a

b

Fig. 4 a – Load/Displacement Curve; b – Resistance Curve

Fig. 4, b known as the "Resistance curve-R curve" is a plot of inter-laminar fracture toughness (G_I-N/m) against crack length (a, mm). Table 3 elaborates on the percentage increase in G_{Ic} for crack initiation. G_{Ic} at crack initiation could be defined as the point of sudden decrease in load as shown in the R-curve. The G_{Ic} was calculated using equation (3). From the curves it's evident that those specimens with CNTs i.e 2.1, 2.2 and 2.3 offered the most resistance to de-lamination as is evident from the increasing inter-laminar fracture toughness. From table 4 it could be inferred that the maximum increase in G_{Ic} was for specimen 2.1 with respect to all the specimens without nanotubes, while in 2.2 and 2.3 it was found to be modest and , in few instances the G_{Ic} dropped to as low as -17.53% as was the case of 2.3 with respect to 1.3. The reason for this increase in only specimen 2.1 couldn't be well understood since *2.n* series were all cut from the same panel. But there was also an increase of 8.52% for 2.2 with respect to 1.1 and 12.83% for 2.2 with respect to 1.2. From these observances it could be hypothesised that some nanotubes in the matrix system may have agglomerated thus preventing the hardening mechanisms like bridging our fibre pull-out from happening, while some may have dispersed more uniformly. But this positive increase in inter-laminar fracture toughness is at the expense of reduced load bearing capacity. The G_{Ic} for crack propagation is another im-

portant aspect to be looked into. It is evident from the R-curve that the inter-laminar fracture toughness during propagation is high in the 2.n series of specimens.

Comparison of G_{Ic} increase in specimens 2.n with respect to specimens 1.n

Specimens G_{Ic}(N/m)	2.1 (855.74)	2.2 (813.23)	2.3 (733.19)
1.1 (749.37)	+14.19%	+8.52%	-2.15%
1.2 (720.71)	+18.73%	+12.83%	+1.73
1.3 (889.14)	-3.75%	-8.53%	-17.53

3.2. Acoustic signals during crack propagation

Wavelet contours where generated using AGU-Vallen Wavelet solver and where classified into Class A denoting matrix cracking, Class B denoting fibre fracture and Class C denoting de-bonding. Table 1 would be used as a reference for this analysis. Group velocities were determined using longitudinal velocity of 2850 m/s and a shear wave velocity of 1980 m/s [16]. The Vallen dispersion solver was used to calculate the group velocities.
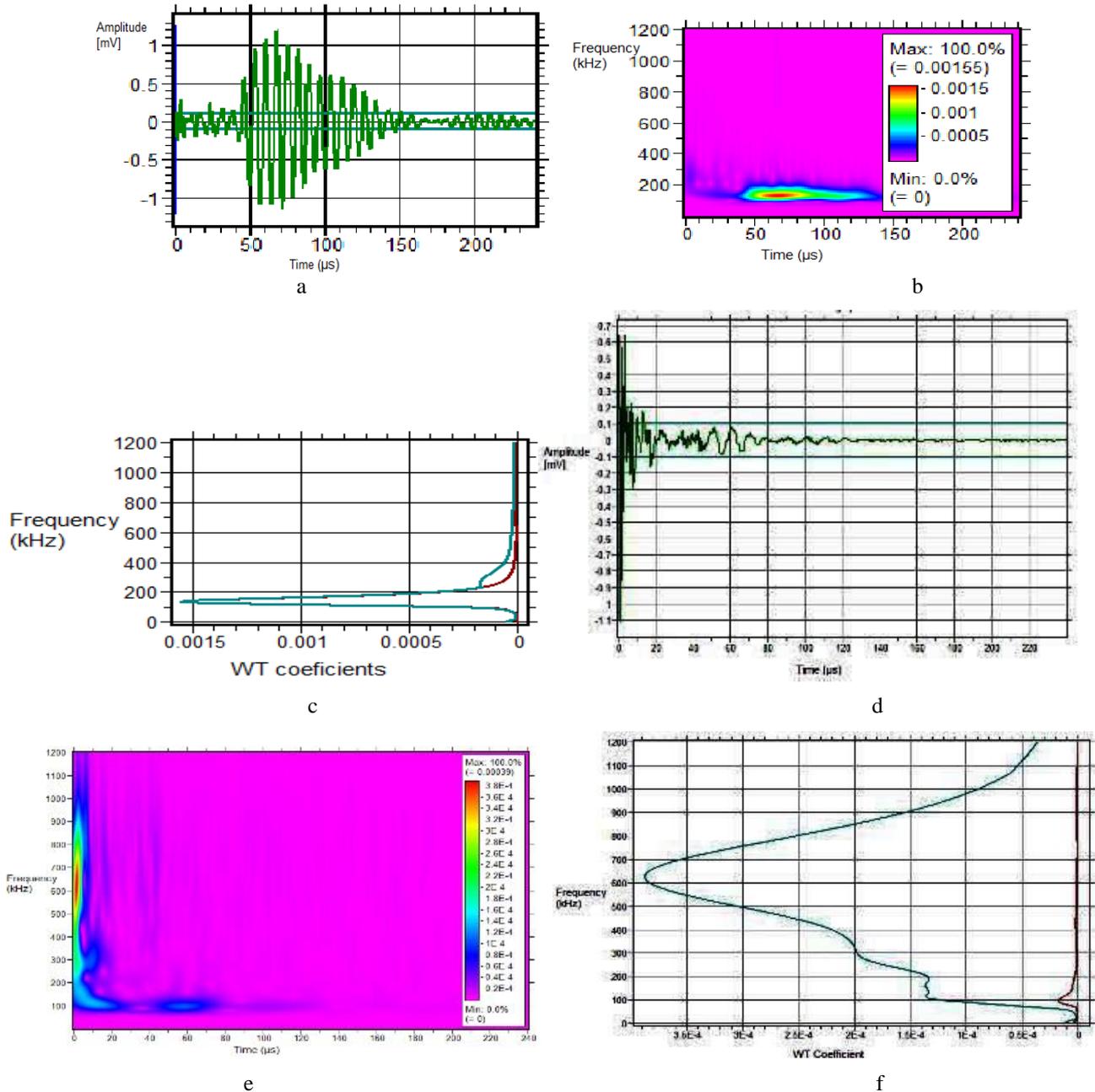
Fig. 5 Waveforms (a), wavelet contours (b) and frequency projections (c) for specimen 1.3 surface matrix crack exciting low frequency A0 mode. Waveform (d), wavelet contour(e) and frequency projections (f) for specimen 2.3, internal matrix crack exciting a high frequency S0 mode

An example of class A is shown below. These waveforms are characterised by slow rise time of approximately 20 μs. In the study conducted in [14] it was found that surface matrix cracks would excite low frequency A0 mode, while an internal crack would excite a high frequency S0 mode. And it has been stated in the same research [14] that AE events at lower stresses are characterised by low frequency corresponding with surface ply cracking and

at high stresses high frequency events are noticed, this was in the context of transverse cracking. The waveforms below (Fig. 5-a, b and c for specimen 1.3) is an example of a low frequency *A0* mode and therefore this waveform could be assigned to that of a surface matrix cracking. From the figure it is clear that the highest concentration of energy is in the *A0* mode at a frequency of 160 kHz at a group velocity of 1.884 m/ms. Peak frequency analysis has also been considered as an accurate way of predicting damage mechanism in composites. Interesting results were found in various studies were it was found that matrix cracking could be attributed to low frequency while fibre breakage to high frequency [14, 17]. If peak frequency analysis was to be considered then the frequency response seen in Fig. 5-a, b and c matches with the frequency found in literature for matrix cracking. Also waveforms that could be assigned to internal matrix cracking i.e. a dominant *S0* mode was obtained in this study. An example is shown below in Fig. 5-d, e and f. Here it is evident that the highest concentration of energy is in the *S0* mode at a frequency of 600 kHz and the group velocity was centred about 1.539 m/ms. This waveform cannot be ascribed to fibre breakage because as per Y.Mizutani et.al [18], fibre breakage should excite high frequency *S0* mode followed by low frequency but high amplitude *A0* modes, these waves would be classed as Class B signals and elaborated next. But our results for Class A contradicts the peak frequency analysis which says that high frequency signals are generated when fibre breaks. From this it can be concluded that the high frequency response for internal matrix cracking and low frequency response for surface matrix crack lies in the modal character of the AE waveforms, therefore peak frequency analysis cannot always point out correctly the failure mechanism within a composite material.

Class B signal here corresponds to fibre breakage. Since the ASTM 5528 standard was followed where the crack opening mode was simulated, no tensile force was applied to the specimen, and hence not many fibre breakages are expected. But still there could be fibre breakage occasionally in the course of the experiment, those few waveforms could be analysed for fibre breakage. In a study conducted by José Martínez-Jequier et'al [11], it was found that the breakage of carbon fibre generated high frequency energy response (*S0* mode) in the range of 300-500kHz. While, if the peak frequency analysis is considered the frequency range for fibre breakage lies between 400-500 kHz [14]. These findings where used as reference for this analysis. Waveforms (a), wavelet contours (b) and frequency projections (c) for specimen 1.3 in the case of fibre breakage is as shown below, Fig. 6. The waveform agrees with the waveform generated for fibre breakage in [18]. Initial high frequency component was followed by low frequency but with high amplitude. Since fibre breakage produces micro-pulses inside the plane, the S0 mode is favoured [11]. From the figure 6 (b) it is evident that there is some energy concentration in the *S0* mode at a frequency of 410 kHz the group velocity was cantered at 2.775 m/ms, while the highest energy concentration is in the *A0* mode at a frequency of 150 kHz, but the group velocity was found to be 1.871 m/ms which is far less when compared to 2.775 m/ms, therefore this should be an *A0* mode. From these observations this waveform could be assigned to fibre breakage. From this observation it's clearer that fibre breakage can excite both *S0* and *A0* modes. Thus,

again it could be stressed that peak frequency analysis can be proved wrong when it states that fibre breakage excites high frequency which was not the case in class A signals. But in the case of fibre breakage both these modes are excited, with a pronounced *S0* mode. But in our case the *S0* mode was not as pronounced as those found in the literature, since there the fibre was subjected to axial tensile force, whereas here it was subjected to bending. Thus, based on these findings along with those mentioned in literature, this waveform shown below could be assigned to that of fibre breakage.

a

b

d
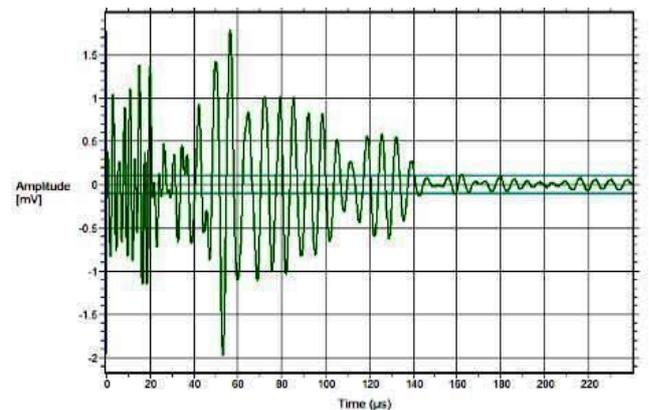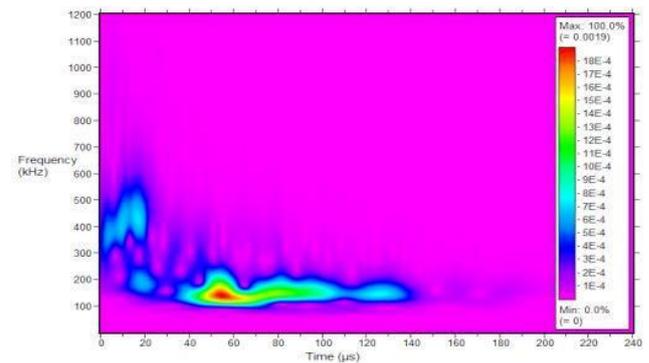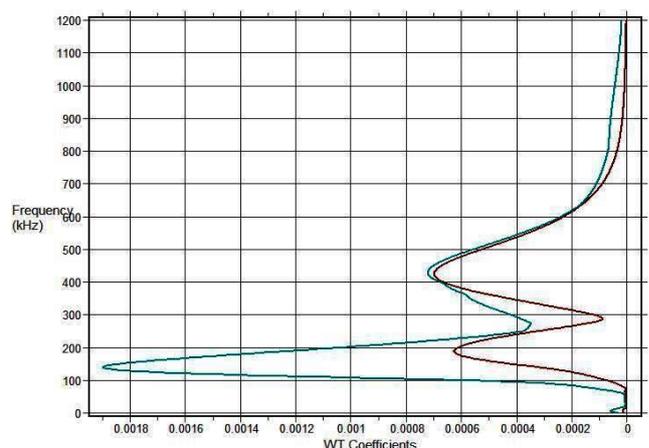
Fig. 6 Waveform (a), wavelet contour (b) and frequency projection (c) for specimen 1.3

Another fracture mechanism observed in fibre reinforced composites is the de-bonding of fibres. Fig. 7 shows de-bonding in specimen 1.3. According to findings

of Y.Mizutani et.al[18], de-bonding excited both *S0* and *A0* mode, with a relatively stronger low frequency *A0* mode. Wavelet contours of specimen 1.3 was studied, and similar results were observed. Here the high frequency *S0* mode was followed by the *A0* mode with comparatively larger amplitudes. The group velocities in both the case centred around 1.8 m/m.
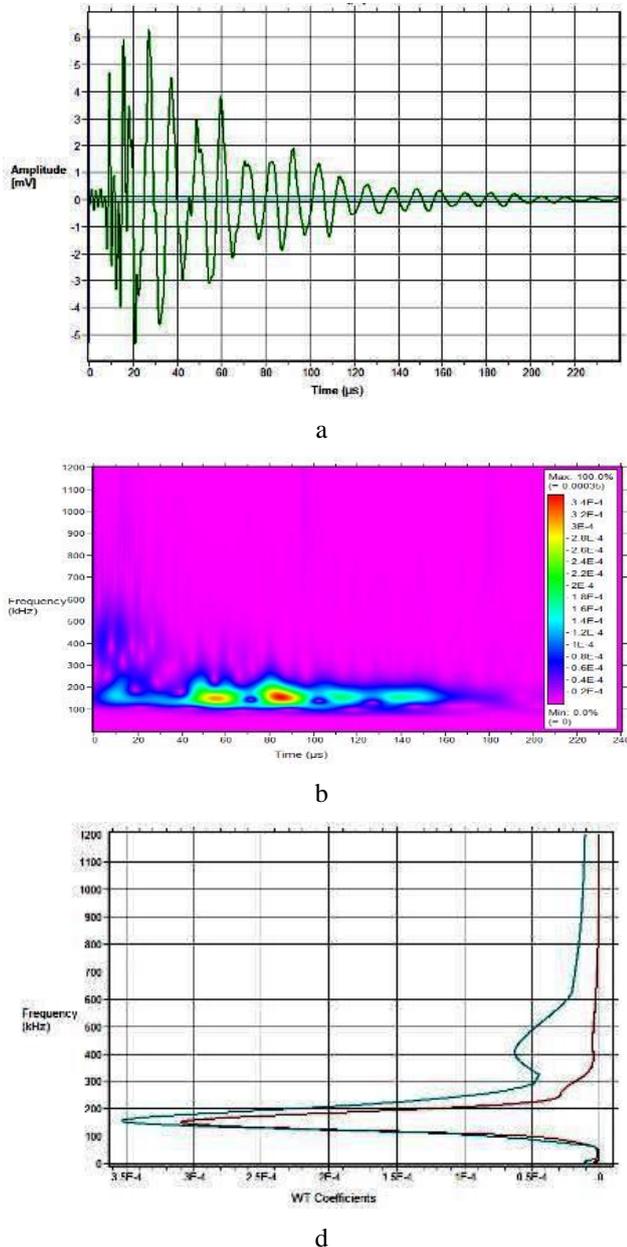

a

b

d

Fig. 7 Waveform (a), wavelet contour (b) and frequency projection (c) for fibre/matrix de-bonding in specimens 1.3

4 Conclusions

The addition of CNTs does had a positive as well as a negative impact on the mechanical properties of the polymer composites. An increase in G_{Ic} was observed in specimens with CNTs, but the percentage increase was far less when compared to those found in literature. Also, the load bearing capacity of the material reduced considerably. But this could be attributed to the way the CNTs where introduced in the specimen. Better results could have been obtained by depositing the CNTs (functionalised) on the

fibre. Acoustic emission methods holds the key to understand the material deterioration in real time. From this study it can also be concluded that the different frequencies, for instance in the case of matrix cracking (surface or internal) and likewise in fibre fracture which was characterised by the presence of both the modes, lie in the modal character of the AE waveforms, and thus associating a single peak frequency with a specific damage might not be an accurate way of predicting damages in a composite material.

References

1. **De Greef, N.; Gorbatikh, L.; Lomov, S.V.; Verpoest, I.** 2011. Damage development in woven carbon fibre/epoxy composites modified with carbon nanotubes under tension in the bias direction, Composites 42: 1635-1644.
   https://doi.org/10.1016/j.compositesa.2011.07.013.
2. **Warrier, A.; Godara, A.; Rochez, O.; Mezzo, L.; Luizi, F,; Gorbatikh, L.; Lomov, S.V.; Versoest, I.** 2010. The effect of adding carbon nanotubes to glass/epoxy composites in the fibre sizing and or the matrix, Composites 41: 532-538.
   https://doi.org/10.1016/j.compositesa.2010.01.001.
3. **De Greef, N.; Gorbatikh, L.; Godara, A.; Mezzo, L.; Lomov, S.V.; Versoest, I.** 2011. The effect of carbon nanotubes on the damage development on in carbon fibre/epoxy composites, Carbon 49: 4650-4664,
   https://doi.org/10.1016/j.carbon.2011.06.047.
4. **Mirjalili, V.; Hubert, P.** 2009. Effect of carbon nanotube dispersion on the fracture toughness of polymers, ICCM-17 17th International Conference on Composite Materials: 27-31.
   http://www.iccm-central.org/Proceedings/ICCM17proceedings/Themes/Nanocomposites/MODELLING%20&%20ANALY%20OF%20NANOCOM/E2.1%20Mirjalili.pdf.
5. **Oskouei, A.R.; Ahmadi**, M. 2009. Acoustic emission characteristics of mode I delamination in glass/polyester composites, Journal of composite material 44: 793-807.
   https://doi.org/10.1177/0021998309349553.
6. **Hojo, M.; Ando, T.; Tanaka, M.; Adachi, T.; Ochiai, S.; Endo, Y**. 2006. Mode I and Mode II interlaminar fracture toughness and fatigue delamination of CF/epoxy laminates with self-same epoxy interleaf, International journal of fatigue 28: 1154-1165.
   https://doi.org/10.1016/j.ijfatigue.2006.02.004.
7. **Perrin, F.; Bureau, M.N.; Denault, J.; Dickson, J.I.** 2003. Mode I interlaminar crack propagation in continuous glass fibre/polypropylene composite: temperature and molding condition dependence, Composite science and technology 63: 597-607.
   https://doi.org/10.1016/S0266-3538(02)00255-5.
8. **R'Milli, M.; Moevus, M.; Godin, N.** 2008. Statistical fracture of E-glass fibres using a bundle tensile and